Genome Biology

RESEARCH

Open Access

H3.3 contributes to chromatin accessibility and transcription factor binding at promoter-proximal regulatory elements in embryonic stem cells

Amanuel Tafessu[†], Ryan O'Hara[†], Sara Martire[†], Altair L. Dube, Purbita Saha, Vincent U. Gant and Laura A. Banaszynski[*]

[†]Amanuel Tafessu, Ryan O'Hara, and Sara Martire contributed equally.

*Correspondence: Laura.Banaszynski@UTSouthwestern.edu

Cecil H. and Ida Green Center for Reproductive Biology Sciences, Department of Obstetrics and Gynecology, Children's Medical Center Research Institute, Harold C. Simmons Comprehensive Cancer Center, Hamon Center for Regenerative Science and Medicine, University of Texas Southwestern Medical Center, Dallas, Texas 75390, USA

Abstract

Background: The histone variant H3.3 is enriched at active regulatory elements such as promoters and enhancers in mammalian genomes. These regions are highly accessible, creating an environment that is permissive to transcription factor binding and the recruitment of transcriptional coactivators that establish a unique chromatin post-translational landscape. How H3.3 contributes to the establishment and function of chromatin states at these regions is poorly understood.

Results: We perform genomic analyses of features associated with active promoter chromatin in mouse embryonic stem cells (ESCs) and find evidence of subtle yet widespread promoter dysregulation in the absence of H3.3. Loss of H3.3 results in reduced chromatin accessibility and transcription factor (TF) binding at promoters of expressed genes in ESCs. Likewise, enrichment of the transcriptional coactivator p300 and downstream histone H3 acetylation at lysine 27 (H3K27ac) is reduced at promoters in the absence of H3.3, along with reduced enrichment of the acetyl lysine reader BRD4. Despite the observed chromatin dysregulation, H3.3 KO ESCs maintain transcription from ESC-specific genes. However, upon undirected differentiation, H3.3 KO cells retain footprinting of ESC-specific TF motifs and fail to generate footprints of lineage-specific TF motifs, in line with their diminished capacity to differentiate.

Conclusions: H3.3 facilitates DNA accessibility, transcription factor binding, and histone post-translational modification at active promoters. While H3.3 is not required for maintaining transcription in ESCs, it does promote de novo transcription factor binding which may contribute to the dysregulation of cellular differentiation in the absence of H3.3.

Keywords: Histone variants, Chromatin accessibility, Transcription factor binding, Embryonic stem cells, Differentiation

Background

In eukaryotic cells, DNA is wrapped around histone proteins to form nucleosomes, the fundamental repeating unit of chromatin [1, 2]. While chromatin functions in part to organize a large amount of genomic material within the confines of the nucleus, the natural consequence of this condensation is that regulatory DNA sequences become masked to transcription factors and other proteins that must locate their target sequences for downstream function [3, 4]. A subset of specialized transcription factors are able to engage nucleosomal DNA, so-called "pioneer" factors [5]. However, many transcription factors must cooperate with chromatin remodeling factors and the local chromatin environment to engage their target DNA sequences [6]. In addition to specific post-translational modifications, nucleosomes at active regulatory elements are enriched with the histone variants H2A.Z and H3.3 [7]. These nucleosomes are proposed to have unique physical properties that may destabilize the nucleosome core particle [8, 9], providing a "window of opportunity" for access to the underlying DNA. Studies of H2A.Z function largely support this view, attributed to both primary sequence differences from replication-coupled H2A and coordinated nucleosome eviction and exchange by dedicated H2A.Z interacting proteins [10–12]. The contribution of H3.3 to chromatin accessibility and transcription factor binding, however, is less clear [13].

H3.3 differs from replication-coupled H3 by only 4–5 amino acids, yet this is sufficient to drive dedicated chaperone association and deposition at specific regions of the genome [7]. H3.3 was first identified as a component of active chromatin [14] and many genome-wide studies have noted its deposition at genic regions such as enhancers, promoters, and gene bodies [15, 16]. Regions of H3.3 deposition are sites of dynamic nucleosome turnover [17–21], and several studies have suggested that H3.3 deposition itself may function to destabilize nucleosomes [8, 22]. However, other studies have found that H3.3 nucleosomes are structurally and thermodynamically indistinguishable from nucleosomes containing canonical H3 [23, 24]. Further, although H3.3 is enriched at active enhancers, previous data show minimal disruption of chromatin accessibility at enhancers in the absence of H3.3, suggesting that H3.3 is correlative with chromatin dynamics rather than causative in this setting [25, 26].

Several studies suggest that H3.3 may influence the local chromatin environment by recruiting specific complexes to chromatin [27–29]. For example, H3.3 recruits chromatin remodeling complexes, particularly SWI/SNF and NuRD, whose role in regulating nucleosome dynamics at regulatory elements may influence transcription factor binding [27, 30]. In addition, H3.3 has been shown to contribute to the post-translational modification (PTM) state found at specific regions [7, 25, 28, 29]. For example, recent studies demonstrate that histone H3 lysine 27 acetylation (H3K27ac), a hallmark of active enhancers and promoters thought to occur downstream of transcription factor binding [13, 31], is reduced in the absence of H3.3 [25, 30, 32]. Perhaps surprisingly, H3.3-mediated reduction of enhancer acetylation is not correlated with global reduction of transcription in mouse embryonic stem cells (ESCs) [25, 33]. However, a number of studies in mammalian cell lines suggest that H3.3 plays a role in de novo transcription [34, 35] in response to extracellular stimuli [25, 36–40], and H3.3 knockout in animal models results in embryonic lethality or sterility [41–43]. Together, these observations suggest that H3.3 may be functionally important to initiate new transcription programs.

In this study, we performed genomic analyses to determine the effect of H3.3 deposition on regulatory element architecture and downstream transcription in ESCs. We find that promoter-proximal regulatory elements become less accessible in the absence of H3.3. Reduced accessibility is accompanied by reduced transcription factor footprinting and binding, attenuation of chromatin states thought to be downstream of transcription factor binding, and decreased RNA polymerase II engagement at affected promoters. While ESCs appear quite tolerant to these changes in genome regulation, they are unable to respond to cellular differentiation cues and show perdurance of the regulatory landscape associated with pluripotency. Thus, we propose that H3.3 is a necessary upstream component of transcriptional activation that becomes dispensable for the maintenance of established gene regulatory networks.

Results

H3.3 increases DNA accessibility at active promoters

Given the dynamic transcription-associated turnover of H3.3 at regulatory elements [20], we wanted to test whether H3.3 is required for accessibility at transcriptionally active regions. We first performed H3.3 chromatin immunoprecipitation followed by sequencing (ChIP-seq) and ATAC-seq on WT ESCs [25]. All ATAC-seq studies were performed in technical duplicate at a minimum sequence depth of 40 million reads for each data set. In agreement with previous studies, we find that H3.3 enrichment at active regulatory elements is correlated with accessibility (Fig. 1A, Additional file 1: Fig. S1A). Accessibility at active promoters (defined as >20 baseMean across WT and H3.3

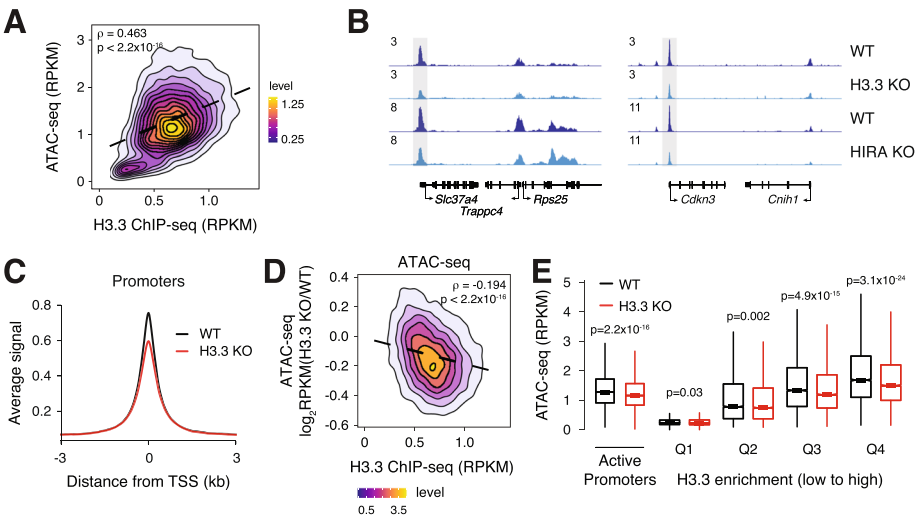

Fig. 1. Loss of H3.3 reduces chromatin accessibility at promoters. **A** Correlation plot between ATAC-seq and H3.3 ChIP-seq at active promoters ($n = 12{,}903$) in ESCs. **B** Genome browser representations of ATAC-seq in WT and H3.3 KO ESCs and WT and HIRA KO ESCs. The *y*-axis represents read density in reads per kilobase per million mapped reads (RPKM). **C** ATAC-seq average profiles at active promoters ($n = 12{,}903$) in WT and H3.3 KO ESCs. **D** Correlation plot between differential ATAC-seq signal in H3.3 KO compared to WT ESCs and H3.3 enrichment at active promoters ($n = 12{,}903$) in WT ESCs. **E** Boxplot showing ATAC-seq signal at active promoters and promoters binned by H3.3 enrichment in WT and H3.3 KO ESCs. The bottom and top of the boxes correspond to the 25th and 75th percentiles, and the internal band is the 50th percentile (median). The plot whiskers correspond to 1.5× interquartile range and outliers are excluded. *p*-values determined by Wilcoxon rank sum two-side test

KO RNA-seq [25], $n = 12{,}903$) showed higher correlation with H3.3 deposition (rho = 0.463) compared to active promoter-distal regulatory elements (defined as regions > 3 kb from the nearest promoter and containing both ATAC-seq and H3K27ac ChIP-seq enrichment, $n = 7972$, rho = 0.2). We next asked whether regulatory element accessibility is dependent upon H3.3 by comparing ATAC-seq data from WT and H3.3 KO ESCs [25, 29]. We observe a slight but significant decrease in chromatin accessibility that is more pronounced at active promoters compared with distal regulatory elements in the absence of H3.3 (Fig. 1B,C and Additional file 1: Fig. S1B-D). Decreased promoter accessibility is apparent both at the level of individual promoters and genome-wide (Fig. 1B,C). We next wanted to determine whether reduced promoter accessibility in H3.3 KO ESCs is related to the level of H3.3 enrichment at that promoter in WT ESCs. Globally, we find that reduced ATAC-seq signal at active promoters in H3.3 KO ESCs is correlated with H3.3 enrichment in WT ESCs (rho = −0.194, Fig. 1D). Further, by binning active promoters into quartiles based on H3.3 enrichment, we observed that promoters with higher H3.3 enrichment indeed showed more pronounced and significant loss of accessibility by ATAC-seq in H3.3 KO ESCs (Fig. 1E).

H3.3 deposition occurs through two distinct chaperone complexes. The HIRA complex is responsible for the majority of H3.3 deposition at promoters, gene bodies, and enhancers, whereas the ATRX–DAXX complex deposits H3.3 at repetitive regions such as telomeres and interstitial heterochromatin [7, 15]. We confirmed that H3.3 deposition was reduced at enhancers and promoters in HIRA KO ESCs compared to WT and that loss of ATRX or DAXX resulted in a slight increase in H3.3 deposition at these regions (Additional file 1: Fig. S2). We therefore predicted that loss of HIRA, but not ATRX or DAXX, would result in similar effects on promoter accessibility as observed upon loss of H3.3. In agreement, we observed a similar reduction in the accessibility of active promoters in HIRA KO ESCs (Fig. 1B, Additional file 1: Fig. S3A-B). By contrast, ATRX KO did not alter regulatory element accessibility and DAXX KO interestingly resulted in a slight increase in chromatin accessibility at both enhancers and promoters (Additional file 1: Fig. S3C-G). Further, we found that genome-wide changes in active promoter chromatin accessibility were correlated in HIRA KO and H3.3 KO ESCs (rho = 0.316) but not in ATRX KO or DAXX KO and H3.3 KO ESCs (rho = 0.071, −0.04 respectively) (Additional file 1: Fig. S3H-J). Active promoters in H3.3 KO ESCs showed higher levels of general H3 deposition compared to WT ESCs, in agreement with the reduced accessibility we observe at these regions (Additional file 1: Fig. S3K). In addition to reduced accessibility, we find that loss of either H3.3 or HIRA, but not ATRX or DAXX, disrupts nucleosome footprinting and positioning at active promoters genome-wide as assessed by NucleoATAC [44] (Additional file 1: Fig. S4). Overall, these data suggest that HIRA-dependent deposition of H3.3 at promoters has a role in maintaining chromatin accessibility and nucleosome organization at these regions.

We next used DiffBind [45] to computationally identify differentially accessible enhancers and promoters in H3.3 KO ESCs (Additional file 1: Fig. S5). Genome-wide, we identified 335 regions of statistically significant differential accessibility at promoters and 632 regions at enhancers in H3.3 KO compared to WT ESCs ($p < 0.05$). Gain and loss of accessibility at enhancers was relatively balanced in the absence of H3.3, with 45% (287/632) of enhancers more accessible and 55% (345/632) less accessible. In

contrast, 79% (265/335) of differentially regulated promoters become less accessible in H3.3 KO ESCs (Additional file 1: Fig. S5A-D). Promoters that became less accessible upon H3.3 KO had higher enrichment of PTMs associated with gene activation (e.g., H3K4me3, H3K27ac) and lower enrichment of PTMs associated with gene silencing (e.g., H3K27me3) in WT ESCs, compared to promoters that became more accessible in H3.3 KO ESCs (Additional file 1: Fig. S5E-G). Both H3.3 deposition and the median expression of genes whose promoters became more closed in the absence of H3.3 was higher than that of expressed genes in ESCs (Additional file 1: Fig. S5H,I). Computationally defined "H3.3-dependent" promoters were also less accessible in HIRA KO ESCs but not in DAXX KO or ATRX KO ESCs (Additional file 1: Fig. S5J). Together, these analyses suggest that highly expressed genes with high levels of H3.3 deposition are dependent upon H3.3 to maintain accessible chromatin at their promoters.

Given the subtlety of the observed reduction of chromatin accessibility at regulatory elements in the absence of HIRA-mediated H3.3 deposition, we sought to further validate our ATAC datasets through assessment of additional genomic regions. Given recent reports demonstrating that repetitive elements show increased accessibility in the absence of ATRX/DAXX-mediated H3.3 deposition [26, 28, 46], we wanted to evaluate accessibility at these regions in our suite of H3.3 KO and chaperone KO ESCs. We first confirmed that intracisternal A-type particles (IAPEz) were more accessible in H3.3 KO compared to WT ESCs (Additional file 1: Fig. S6A). This was also the case in ATRX KO ESCs and DAXX KO ESCs (Additional file 1: Fig. S6B,C). However, we observe no change in chromatin accessibility at these regions in the absence of HIRA (Additional file 1: Fig. S6D). In summary, while global loss of H3.3 results in changes in chromatin accessibility at both regulatory elements and repetitive elements, reduced chromatin accessibility in HIRA KO ESCs is primarily restricted to regulatory elements, whereas increased chromatin accessibility in ATRX or DAXX KO ESCs is most obviously apparent at repetitive elements.

H3.3 facilitates transcription factor binding at promoters

Given that chromatin accessibility is a hallmark of regulatory element TF binding, we hypothesized that the reduced promoter accessibility observed in H3.3 KO and HIRA KO ESCs would be accompanied by reduced TF binding. ATAC-seq data measures chromatin accessibility but also contains regions of depleted signal within open chromatin that are protected from transposition by TF binding, referred to as TF footprints. We used a recently developed tool called TOBIAS [47] to perform comparative footprinting analysis of 395 expressed TFs with known consensus motifs in WT and H3.3 KO ESCs. This analysis revealed that nearly all expressed TFs show reduced footprinting in the active promoters of H3.3 KO ESCs, including key members of the TF network that controls pluripotency, POU5F1 (e.g., Oct4), Sox2, and Nanog [48] (Fig. 2A, Additional file 1: Fig. S7, Additional file 2: Table S1). Analysis of ATAC-seq data centered on select pluripotency TF motifs showed clearly reduced accessibility upon loss of H3.3 (Fig. 2B). While all TFs show reduced binding scores in the absence of H3.3, those families most affected based on the magnitude and significance of dysregulation bind to motifs containing high GC content (Fig. 2C, Additional file 1: Fig. S5K), perhaps reflective of their presence at promoters. In line with our accessibility analysis, DAXX KO and ATRX KO

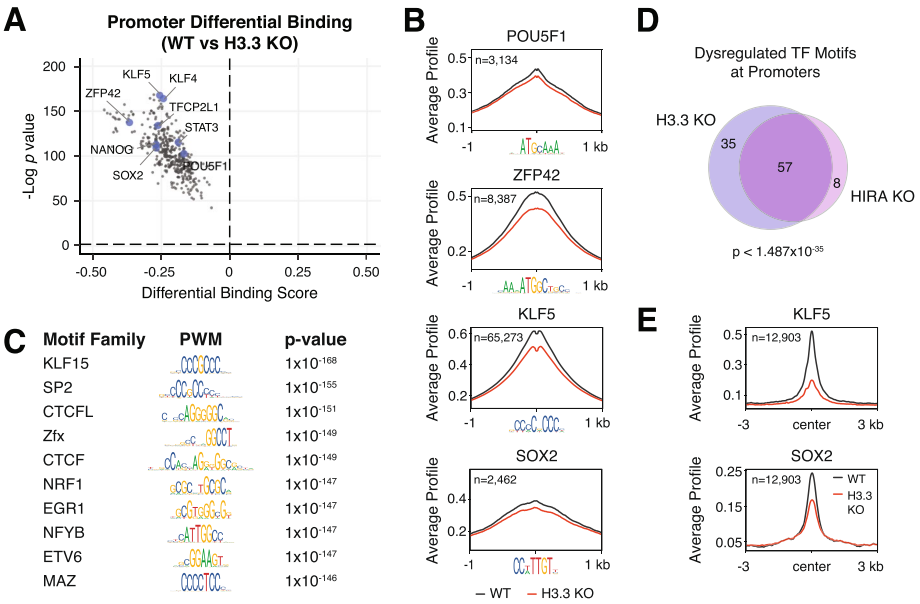

Fig. 2. Loss of H3.3 reduces TF footprinting at promoters. **A** Pairwise comparison of TF activity at active promoters ($n = 12{,}903$) between WT and H3.3 KO ESCs. The volcano plot shows differential binding activity against the −log10(p-value) for all investigated TF motifs. Each TF is represented by a single circle ($n = 395$). TF motifs enriched in WT ESCs have negative differential binding scores and TF motifs enriched in H3.3 KO ESCs have positive differential binding scores. Motifs for a subset of pluripotency-associated TFs are highlighted in blue. **B** ATAC-seq average profiles at representative TF motifs at promoters in WT and H3.3 KO ESCs. Data are centered on the motif, and the number of motifs profiled is indicated. **C** Illustration of motifs of the most dysregulated TF families at promoters in H3.3 KO ESCs classified based on Manhattan scores in the top 10% across all comparisons (i.e., WT vs H3.3 KO, HIRA KO, ATRX KO, or DAXX KO). **D** Venn diagram representing TF motifs commonly dysregulated at promoters in H3.3 KO and HIRA KO ESCs based on Manhattan score as described above. **E** CUT&Tag average profiles of KLF5 (top) and SOX2 (bottom) enrichment at active promoters (n=12,903) in WT and H3.3 KO ESCs. Three kilobases around the center of promoters are displayed for each analysis

ESCs did not substantially affect TF binding at promoters but did result in increased TF binding at IAPEz repeat elements (Additional file 1: Fig. S8, Additional file 1: Fig. S9A-D, Additional file 2: Table S1). In contrast, HIRA KO ESCs showed a similar reduction of TF binding at active promoters as that observed in H3.3 KO ESCs (Additional file 1: Fig. S8, Additional file 2: Table S1). As expected, the most highly dysregulated TF families in H3.3 KO and HIRA KO ESCs overlap significantly (Fig. 2D).

Since ATAC-seq footprinting is a proxy for TF binding, we wanted to confirm these results using antibody-based methods to assess TF enrichment at promoters in WT and H3.3 KO ESCs. We chose Sox2 and Klf5 as representative TFs for assessment, based on the role of Sox2 in pluripotency and the GC content of the Klf5 motif. Analysis of CUT&Tag [49] data confirmed that both Sox2 and Klf5 enrichment at promoters was reduced in the absence of H3.3 (Fig. 2E, Additional file 1: Fig. S9E-H). Likewise, TF binding at IAPEz elements was increased in H3.3 KO ESCs (Additional file 1: Fig. S9E-H).

Reduced TF binding in H3.3 and HIRA KO ESCs could be caused either by altered binding ability or by reduced TF expression. When we compared published RNA-seq data for WT, H3.3 KO, and HIRA KO ESCs [25], we did not observe widespread decrease in TF expression in either H3.3 KO or HIRA KO ESCs (Additional file 1: Fig. S10A,B; Additional file 3: Table S2). Further, we found no correlation between changes

in TF expression and differential TF binding scores due to loss of H3.3 or HIRA (Additional file 1: Fig. S10C,D). Finally, we do not observe changes in expression at the protein level for a subset of assessed pluripotency TFs in H3.3 KO compared to WT ESCs (Additional file 1: Fig. S10E). Together, our results suggest that loss of H3.3 deposition does not affect TF levels but rather affects the ability of TFs to bind to promoters.

Dysregulation of promoter chromatin landscape in the absence of H3.3

Promoters of active genes contain distinct chromatin post-translational modifications. These regions are enriched with H3K27ac and H3K4me3, deposited by the CBP/p300 acetyltransferases and the MLL1/2 methyltransferases, respectively [50, 51]. Recruitment of these enzymes has been shown to be downstream of TF binding [13, 52–55]. CBP/p300-mediated histone acetylation in turn acts as a scaffold to recruit effector proteins such as the bromodomain and extra-terminal domain (BET) family protein BRD4, which is involved in transcription elongation [56]. Given the reduction in both accessibility and TF binding observed at promoters lacking H3.3, we hypothesized that subsequent steps in establishing the promoter chromatin landscape may be dysregulated.

To explore the relationship between H3.3 deposition and chromatin signatures at promoters, we both reanalyzed existing data sets [25] and performed additional ChIP-seq of several modifications and chromatin-associated proteins in WT and H3.3 KO ESCs. Genome-wide, we observed a subtle decrease in H3K4me3 at active promoters (Fig. 3A,B, Additional file 1: Fig. S11A,E). Interestingly, the molecular machinery associated with histone acetylation appears more greatly dependent on H3.3. We find that loss of H3.3 leads to reduced enrichment of p300, H3K27ac, and BRD4 at active promoters genome-wide (Fig. 3A,C–E, Additional file 1: Fig. S11B-D). Reduced enrichment of each factor in H3.3 KO ESCs was correlated with the level of H3.3 enrichment present at promoters in WT ESCs (Additional file 1: Fig. S11F-H) and clearly apparent at the "H3.3-dependent" promoters ($n = 265$) identified as differentially accessible in the absence of H3.3 (Additional file 1: Fig. S11I-L). The effect of H3.3 loss on p300, H3K27ac, and BRD4 was not restricted to promoters containing specific TF motifs, but rather appeared more global, with even regions bound by lineage-drivers such as Oct4, Sox2, and Nanog showing reduced enrichment (Fig. 3F, Additional file 1: Fig. S11M). Reduced recruitment of p300 and BRD4 at promoters cannot be attributed to reduced expression of these genes in H3.3 KO ESCs (Additional file 1: Fig. S10), suggesting that the presence of H3.3 itself plays a role in stabilizing these proteins at active promoters.

Finally, since H3.3 deposition at promoters is facilitated by the HIRA complex, we again expect that loss of HIRA, but not ATRX or DAXX, will phenocopy the effects of loss of H3.3 at promoters. As proof-of-principle, we reanalyzed existing H3K27ac ChIP-seq data sets obtained from WT, HIRA, ATRX, or DAXX KO ESCs [25]. In agreement with our ATAC-seq results, we find that only loss of HIRA resulted in reduced H3K27ac at active promoters compared to WT ESCs (Additional file 1: Fig. S11N). In contrast, loss of ATRX had no effect on promoter H3K27ac enrichment while loss of DAXX resulted in a slight increase in H3K27ac at active promoters (Additional file 1: Fig. S11O,P). This effect was clear when directly comparing the ratio of H3K27ac enrichment at individual promoters in WT and H3.3 chaperone KO ESCs (Additional file 1: Fig. S11Q). Overall, our data demonstrate that HIRA-dependent H3.3 deposition positively influences p300

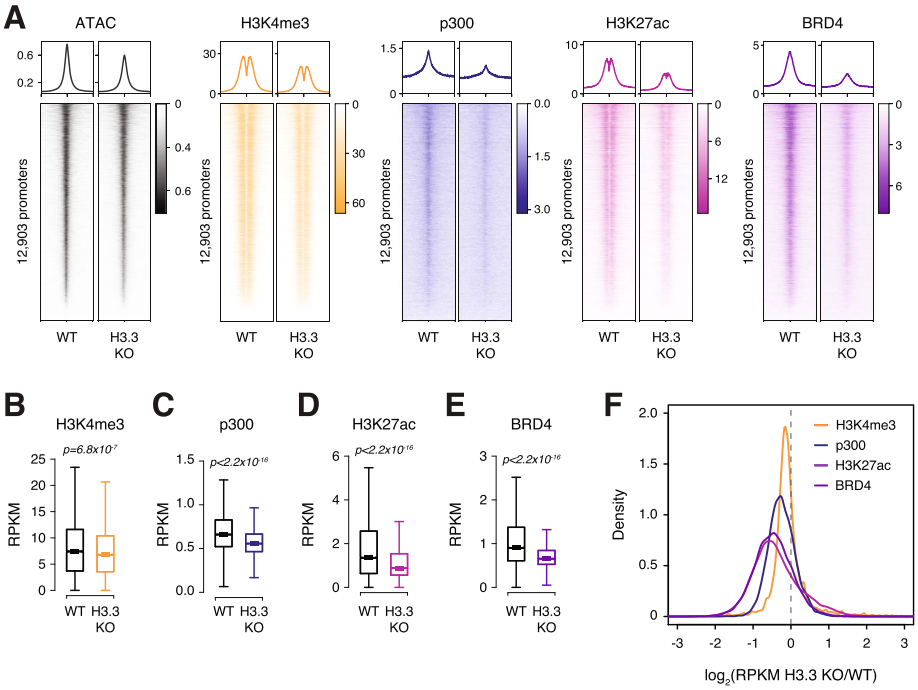

Fig. 3. Chromatin landscape is dysregulated with H3.3 loss. **A** Average profiles (top) and heatmaps (bottom) of ATAC-seq, H3K4me3, p300, H3K27ac, and BRD4 enrichment at active promoters ($n = 12{,}903$) in WT and H3.3 KO ESCs. Three kilobases around the center of promoters are displayed for each analysis. **B–E** Boxplots showing **B** H3K4me3, **C** p300, **D** H3K27ac, and **E** BRD4 enrichment at active promoters in WT and H3.3 KO ESCs ($n = 12{,}903$). The bottom and top of the boxes correspond to the 25th and 75th percentiles, and the internal band is the 50th percentile (median). The plot whiskers correspond to 1.5× interquartile range and outliers are excluded. *p*-values determined by Wilcoxon rank sum two-side test. **F** Ratio (log2) of H3K4me3, p300, H3K27ac, and BRD4 enrichment at active promoters ($n = 12{,}903$) in WT and H3.3 KO ESCs. *x*-axis values <0 indicate reduced enrichment in the absence of H3.3

binding, H3K27 acetylation, and recruitment of downstream effectors such as BRD4 at promoters.

Reduced promoter RNA polymerase II engagement in H3.3 KO cells

Our results demonstrate that active promoters lacking H3.3 show reduced enrichment of histone modifications and cofactors characteristic of transcriptional activity (Fig. 3), suggesting that this activity may be reduced in the absence of H3.3. To test whether loss of these marks was associated with reduced active RNA polymerase II (RNAPII) engagement, we performed global run-on sequencing (GRO-seq) from WT and H3.3 KO ESCs. This technique relies on the strong interaction between transcriptionally engaged RNAPII and DNA to produce nascent transcripts in vitro that are then sequenced and mapped to determine sites of active RNAPII within the genome [57]. In agreement with dysregulation of the chromatin landscape at active promoters, we find that active RNAPII engagement was reduced at the TSS of expressed genes in H3.3 KO compared to WT ESCs (Fig. 4A, Additional file 1: Fig. S12). Interestingly, the change in GRO-seq signal at individual promoter-proximal TF motifs in H3.3 KO compared to WT ESCs was correlated with reduced footprinting of that TF in H3.3 KO ESCs, suggesting an

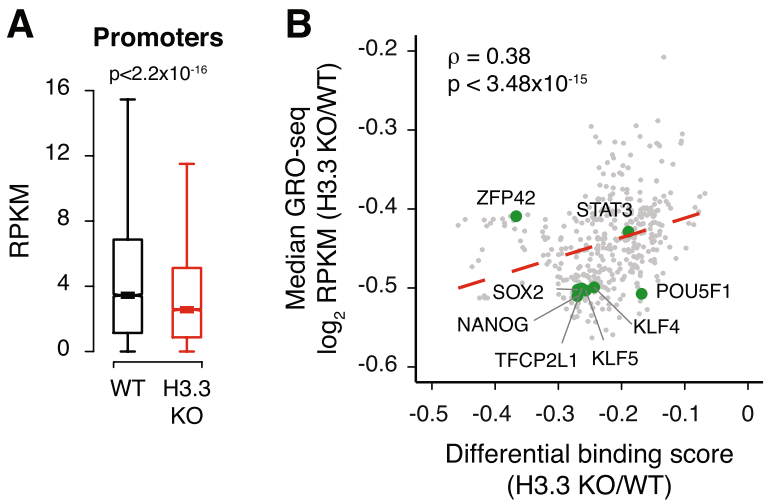

Fig. 4. H3.3 facilitates active RNAPII engagement at promoters. **A** Box plot showing GRO-seq signal at promoters of expressed genes (TSS − 30 bp to TSS + 250 bp) in WT and H3.3 KO ESCs. The bottom and top of the boxes correspond to the 25th and 75th percentiles, and the internal band is the 50th percentile (median). The plot whiskers correspond to 1.5× interquartile range and outliers are excluded. *p*-values determined by Wilcoxon rank sum two-side test. **B** Scatterplot showing differential binding scores of investigated TF motifs and median ratio (log2) of GRO-seq signal at promoters containing each motif. Each TF is represented by a single dot ($n = 395$). Representative TF motifs are labeled in green. Dashed red line represents a linear fit

association between the magnitude of TF dysregulation and the reduction of RNAPII engagement (Fig. 4B).

H3.3 is required for de novo TF activity

Surprisingly, loss of RNAPII engagement observed in H3.3 KO ESCs is not associated with a global reduction in steady-state transcription, as measured by RNA-seq [25]. Although we do observe differentially expressed genes by RNA-seq, the core ESC transcriptional program remains mostly unperturbed. Of the 335 genes that constitute the "core ESC-like gene module" [58], only 8 genes show >2-fold reduced expression in H3.3 KO ESCs (Additional file 1: Fig. S13A). Similarly, expression of the PluriNet protein-protein network characteristic of pluripotent cells [59] is maintained in the absence of H3.3 (Additional file 1: Fig. S13B). Thus, although RNAPII engagement is reduced in the absence of H3.3, the remaining RNAPII appears sufficient for maintaining the ESC transcriptome.

While H3.3 KO ESCs maintain their ability to self-renew, we previously reported that H3.3 is required for undirected differentiation of ESCs into embryoid bodies (EBs) [25]. This process requires both the decommissioning of the existing transcription program as well as the establishment of new gene regulatory networks driven by lineage-specific TFs [60]. H3.3 KO ESCs show a defect in EB formation [25] accompanied by failure to downregulate ESC-specific genes (Additional file 1: Fig. S13C-E). Given the reduced TF binding scores observed in H3.3 KO ESCs, we hypothesized that H3.3 may be involved in the establishment of new lineage-specific TF binding during EB formation.

The complex mixture of cell types present in EBs poses a challenge for TF footprint analysis. To test whether our approach can distinguish between ESC and EB-specific TF footprinting, we generated ATAC-seq data sets from WT ESCs and WT cells differentiated for 4 days into EBs and performed footprint analysis using TOBIAS [47]. Using our previously published EB and ESC RNA-seq data [25], we compiled a list of 458 TFs which were expressed in either EB or ESCs, including 63 EB-specific and 16 ESC-specific TFs. Since we were specifically interested in the effect of H3.3 loss on the decommissioning of ESC genes and on the activation of EB transcriptional programs, we restricted our analysis to promoters which were expressed specifically in either cell state, resulting in 8389 ATAC-seq peaks that were unique to either EBs or ESCs. As expected, TF motifs characteristic of pluripotent cells (e.g., KLF4, NANOG, and SOX2) were more bound in ESCs, whereas lineage-specific TFs (e.g., FOXA2, GATA2, HAND2) had greater footprinting in EBs (Fig. 5A, Additional file 4: Table S3). This result gave us confidence that we could distinguish between EB and ESC-specific footprinting.

To determine whether loss of H3.3 was associated with failure to establish new patterns of TF binding during differentiation, we performed ATAC-seq on WT and H3.3 KO EBs and compared TF footprinting at cell state-specific ATAC-seq peaks. In agreement with the failure of H3.3 KO cells to properly form EBs, our analyses revealed that pluripotency-maintaining TFs tended to remain bound to their motifs (e.g., POU5F1, NANOG, and ZFP42) in H3.3 KO EBs, suggesting an inability to decommission ESC-specific binding patterns. Likewise, lineage-specific TFs (e.g., HAND2, GATA3, and TWIST2) show greater binding in WT EBs, suggesting a defect in initiating differentiation-specific binding events in H3.3 KO cells (Fig. 5B, Additional file 4: Table S3).

While some lineage-specific TFs are upregulated upon differentiation in H3.3 KO cells, many TFs are not expressed to the level observed in WT differentiating cells, reflective of the general failure of H3.3 KO cells to differentiate into EBs (Additional file 1: Fig. S13F). Though it is possible that altered TF binding plays a role in the observed differentiation defect, it is difficult to disentangle defects in TF binding from the transcriptional

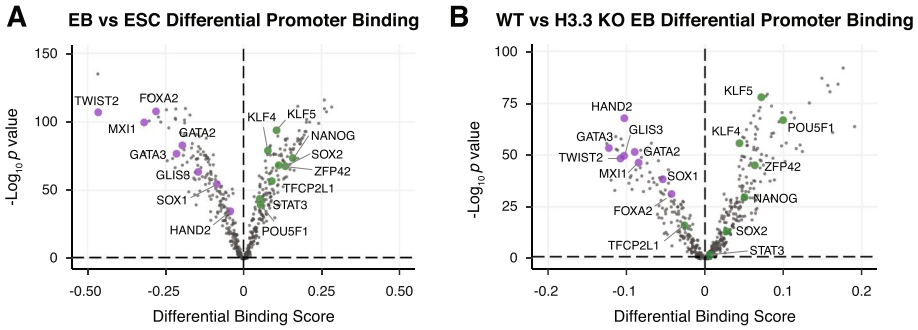

Fig. 5. H3.3 supports TF binding during differentiation. **A** Pairwise comparison of TF activity at promoters between WT ESCs and EBs. TF motifs enriched in EBs have negative differential binding scores and TF motifs enriched in ESCs have positive differential binding scores. **B** Pairwise comparison of TF activity at promoters between WT and H3.3 KO EBs. TF motifs enriched in WT EBs have negative differential binding scores and TF motifs enriched in H3.3 KO EBs have positive differential binding scores. For both panels, the volcano plot shows differential binding activity against the −log10(*p*-value) for all investigated TF motifs. Each TF is represented by a single circle ($n = 458$). Representative differentiation-specific TFs are labeled in purple and representative pluripotency-specific TFs are labeled in green

differences in TF expression. To directly test the ability of H3.3 to facilitate TF binding required during induced transcriptional states (such as differentiation), we developed a model in which Flag-tagged TFs were expressed de novo under the control of a doxycycline-inducible promoter in the presence or absence of H3.3. Using this system, we performed anti-Flag CUT&Tag for three different TFs which are normally very lowly or not expressed in ESCs (i.e., BHLHA15, HAND2, and TWIST2). Upon doxycycline treatment, all TFs are robustly expressed in both WT and H3.3 KO ESCs, with even higher protein levels observed in the absence of H3.3 (Fig. 6A–C, Additional file 1: Fig. S14). Despite this, and in line with our ATAC-seq and CUT&Tag data of endogenous factors, we see that BHLHA15, HAND2, and TWIST2 show reduced binding at promoters in H3.3 KO ESCs (Fig. 6D–F, Additional file 1: Fig. S15). While the majority of TF binding occurs at a subset of already accessible promoters, H3.3-dependent binding is observed at regions of closed chromatin, as well (Additional file 1: Fig. S15). Taken together, our analyses suggest that while H3.3-mediated TF binding may not be required to maintain gene regulatory networks in ESCs, H3.3 deposition likely plays an essential role in establishing new TF binding patterns such as those required for differentiation due to both direct effects of H3.3 on TF binding and indirectly by providing accessible chromatin in pluripotent cells that promotes lineage-specific factor binding.

Discussion

The specific contribution of H3.3 to the establishment and maintenance of transcriptionally permissive chromatin remains an open question. Our genomic studies have revealed a relationship between H3.3 deposition and accessibility of active promoters in ESCs. Our data suggest a role for H3.3 in facilitating TF binding to these regions, as well as maintenance of histone modifications and cofactors associated with transcriptionally active genes, including RNAPII engagement. H3.3 KO ESCs are able to maintain

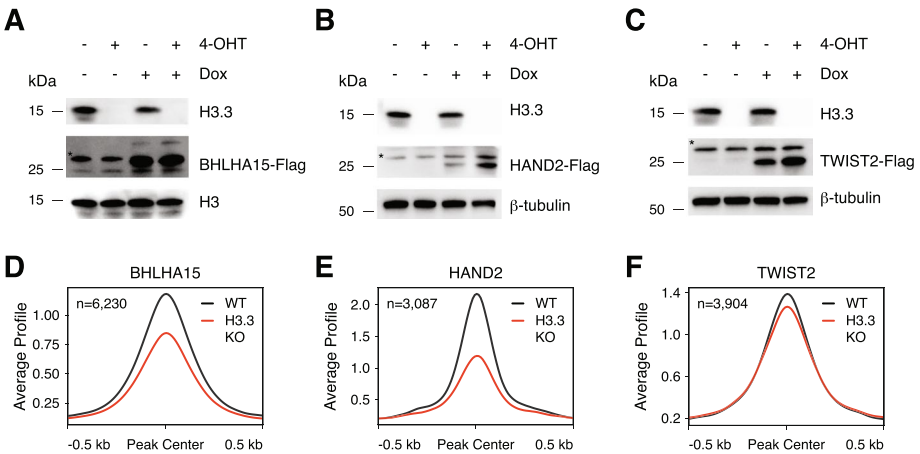

Fig. 6. H3.3 promotes binding of de novo expressed TFs. **A–C** Immunoblot of whole cell lysates from *H3f3a*$^{fl/fl}$;*H3f3b*$^{fl/fl}$;*GtROSA26*$^{CRE\text{-}ERT2}$ ESCs treated with either EtOH or 2 μM 4-Hydroxytamoxifen for 48 h followed by treatment with either DMSO or 0.5 μg/ml doxycycline for 48 h showing expression levels of H3.3 and Flag-tagged **A** BHLHA15, **B** HAND2, or **C** TWIST2. *Non-specific band ~30 kDa observed in all lysates. Total histone H3 or β-tubulin are used as loading controls. **D–F** CUT&Tag average profiles of **D** BHLHA15-Flag, **E** HAND2-Flag, and **F** TWIST2-Flag at promoter-proximal regions enriched in WT ESCs in WT and H3.3 KO ESCs. Three kilobases around the center of promoters are displayed for each analysis, and the number of regions profiled is indicated

transcription despite global, albeit modest, dysregulation of chromatin architecture at promoters. In contrast, loss of H3.3 has dramatic consequences on EB differentiation which coincides with widespread failure to engage lineage-specific TF motifs, along with reduced binding of de novo expressed TFs. Taken together, our data suggests distinct roles for H3.3 in the maintenance of and initiation of transcription.

While the features of active regulatory elements are well-characterized, the order of events that generate transcriptionally permissive chromatin landscapes remains poorly understood. The binding of pioneer TFs to nucleosomal DNA is thought to initiate the assembly of chromatin-modifying protein complexes at promoters [5, 25]. However, even pioneer TFs have been shown to be sensitive to nucleosome composition and reliant on specific chromatin remodeling complexes. For instance, the recruitment of OCT4, a model pioneer TF [61, 62], is facilitated both by H2A.Z and BAF complex recruitment in ESCs [11, 63]. Further, the BAF complex has been shown to facilitate reprogramming of somatic cells to induced pluripotent stem cells (iPSCs) by enhancing OCT4 binding to target sequences [64]. In our assessment, both pioneer factors as well as TFs that are dependent on chromatin remodeling complexes [65] were affected by loss of H3.3 in ESCs, suggesting that this replacement variant is broadly required for optimal TF binding to DNA. Of note, the three de novo TFs which we demonstrate to rely on H3.3 for binding are all members of the basic helix-loop-helix (bHLH) family. In the future, it will be important to perform comprehensive studies assessing whether specific TF features dictate reliance on H3.3 for optimal binding. Interestingly, a previous study reported that depletion of H3.3 early in reprogramming facilitates the repression of somatic genes; however, H3.3 deposition at later time points was required to initiate ESC-like transcription [66]. These observations are in line with our own and suggest a dual role for H3.3 in both safeguarding cellular identity but also facilitating new transcription during cell fate transitions.

Previous studies have shown that HIRA-dependent H3.3 deposition at promoters proceeds via a gap-filling mechanism to protect the transiently naked DNA that is exposed in the wake of RNAPII transcription [17, 21]. One interpretation of our results is that H3.3 itself is necessary for nucleosome displacement to occur. It is also possible that the effects we observe are due to a rapid cell cycle (ESCs double every 12–18 h) and ample access to replication-associated H3.1/2 resulting in higher nucleosome occupancy at regulatory elements. Regardless, reduced access to underlying DNA in the absence of H3.3 then results in reduced recruitment of TFs to their target motifs, setting off a cascade of events resulting in reduced p300 recruitment with subsequent downregulation of H3K27ac at promoters. While this seems plausible at promoters, it is important to note that phosphorylation of a unique serine on the H3.3 tail (substituted by an alanine in replication-coupled H3) has been shown to stimulate p300 activity and H3K27ac at both enhancers and promoters [25, 32]. In contrast to what we see at promoters, loss of H3K27ac at enhancers occurs without any appreciable decrease in p300 recruitment and minimal changes in chromatin accessibility [25], suggesting that distal regulatory elements may be subject to distinct mechanisms of control in ESCs.

Recent studies have shown that loss of histone post-translational modifications long associated with active enhancers and promoters has little effect on ongoing transcription [25, 33, 67, 68], with several studies suggesting that histone-modifying enzymes play

noncatalytic roles in transcription [69–72]. In line with these findings, we observed that H3.3 KO ESCs were largely able to maintain their transcription program and cell identity despite reduced H3K27ac enrichment at promoters. However, we and others have previously shown a requirement for H3.3 during differentiation [25, 30]. In the current study, we showed that loss of H3.3 results in reduced footprinting of lineage-specific TFs and a failure to disengage master ESC regulators during differentiation. Interestingly, proper ESC differentiation requires enhancer decommissioning by the H3K4/K9 demethylase LSD1 [73], a component of the NuRD complex which has been shown to be recruited by H3.3 [27, 73]. Thus, it is possible that the persistence of ESC-specific TF networks we observed in H3.3 KO EBs is due to a failure to decommission active enhancers in addition to an inability to recruit TFs to lineage-specific regulatory elements. It is also possible that the inherent heterogeneity of embryoid body differentiation masks underlying mechanisms of transcription program initiation and decommissioning that might be more apparent under directed conditions, such as differentiation to neuronal precursors or cardiomyocytes.

Interestingly, H3.3 has previously been shown to facilitate the recruitment of both BAF and NuRD complexes in a manner that requires the H3.3 K4 residue [27, 30]. Given the widespread reliance of TFs on chromatin remodeling, it is possible that this function of H3.3 underlies the extensive TF dysregulation we observe in H3.3 KO ESCs. It remains to be seen whether mutation of specific H3.3 residues or deletion of specific chromatin remodelers can recapitulate loss of chromatin accessibility and TF binding that we observe in H3.3 KO ESCs. Future studies investigating the activities of specific remodelers in the absence or mutation of H3.3 will shed light on how H3.3 influences chromatin dynamics and transcriptional regulation.

Conclusions

In this study, we investigated the contributions of histone H3.3 to chromatin states at promoters. Using genomic analyses, we find that H3.3 promotes accessibility, TF binding, and the enrichment of transcriptional coactivators p300 and BRD4 at active promoters. Active RNAPII and histone acetylation associated with active promoters are also depleted in the absence of H3.3, with seemingly no global effect on steady-state transcription. However, in agreement with previous reports, we find that H3.3 is important for gene regulation during differentiation. Specifically, H3.3 is required for the rewiring of TF networks observed during lineage commitment, and for the binding of de novo expressed TFs. Our findings build on previous work linking H3.3 deposition to gene activation and identify a role for H3.3 in maintaining transcriptionally permissive chromatin. Given that H3.3 mutations have been identified in pediatric cancers and congenital neurologic disorders, our studies on normal H3.3 function have important implications towards understanding how dysregulation of this histone variant influences human disease [74–76].

Methods

ESC culture

ESCs were maintained under standard conditions on gelatin-coated plates at 37 °C and 5% CO_2, in medium containing Knockout DMEM (Thermo Fisher) supplemented with

NEAA, GlutaMAX, penicillin/streptomycin (Thermo Fisher), 10% ESC-screened fetal bovine serum (Hyclone), 0.1 mM 2-mercaptoethanol (Fisher), and leukemia-inhibitory factor (LIF). Generation of H3.3 KO, ATRX KO, DAXX KO, and HIRA KO ESCs has been described previously [25, 29, 77]. Feeder-free male H3.3 KO ESCs are a mixed 129xC57BL/6JxICR background. Feeder-free male ATRX, DAXX, and HIRA KO ESCs are a mixed C57BL/6x129Sv background. Feeder-free female inducible H3.3 KO ESCs are *H3f3a*$^{fl/fl}$;*H3f3b*$^{fl/fl}$;*GtROSA26*$^{CRE\text{-}ERT2}$ on a mixed C57BL/6xFVB background. The piggybac transposon system was used to stably integrate transgenic Flag-tagged TFs under control of an rtTA promoter (Systems Biosciences, PB-TRE-EGFP-EF1a-rtTA) into the inducible H3.3 KO ESCs. H3.3 KO was induced by treatment with 2 μM 4-Hydroxytamoxifen for 48 h. TF expression was induced by treatment with 0.5 μg/ml doxycycline for 48 h, at which point cells were harvested for immunoblot and CUT&Tag. ESCs were routinely screened for mycoplasma. For EB formation, ESCs were diluted to 10^4 cells/ml in EB differentiation media (DMEM, 15% FBS, 1× MEM-NEAA, 1× Pen/Strep, 50 μM β-mercaptoethanol) and 30-μl drops were placed on the lid of a 150-mm dish. The lid was inverted and placed over a dish containing 10–15 ml of PBS. The hanging drops were cultured for 3 days at 37 °C and 5% CO_2. The hanging drops were then washed from the lids with EB differentiation media and cultured in 100-mm dishes on an orbital shaker at 50 rpm for an additional day.

Antibodies

The antibodies were as follows: Brd4 (A301-985A50, Bethyl), H3 general (ab1791, Abcam, Lot # GR177884-2), H3.3 (09-838, Millipore, Lot # 2578126), H3K4me3 (39159, Active Motif), Spike-In antibody (61686, Active Motif, Lot# 00419007), OCT4 (sc-5279, Santa Cruz), NANOG (ab70482, Abcam), KLF4 (ab34814, Abcam), KLF5 (61099, Active Motif), SOX2 (AF2018, R&D Systems), Flag (2368, Cell Signaling), β-tubulin (T5201, Sigma), anti-mouse IgG-HRP (NA93V, GE, Lot # 9773218), anti-rabbit IgG-HRP (170-6515, Biorad, Lot # 350003248).

Chromatin immunoprecipitation (ChIP)

Native ChIP

Cells were trypsinized, washed, and lysed (50 mM TrisHCl pH 7.4, 1 mM $CaCl_2$, 0.2% Triton X-100, 10 mM NaButyrate, and protease inhibitor cocktail (Roche)) with micrococcal nuclease (Worthington) for 5 min at 37 °C to recover mono- to tri-nucleosomes. Nuclei were lysed by brief sonication and dialyzed twice into RIPA buffer (10 mM Tris pH 7.6, 1 mM EDTA, 0.1% SDS, 0.1% Na-Deoxycholate, 1% Triton X-100) for 1 h at 4 °C. Soluble material was combined with 50 ng spike-in chromatin (Active Motif 53083) and 5% was reserved as input DNA. Five micrograms of antibody and 2 μg of spike-in antibody (Active Motif 61686) were bound to 50 μl protein A or protein G Dynabeads (Invitrogen) and incubated with soluble chromatin overnight at 4 °C. Magnetic beads were washed as follows: 3× RIPA buffer, 2× RIPA buffer + 300 mM NaCl, 2× LiCl buffer (250 mM LiCl, 0.5% NP-40, 0.5% Na-Deoxycholate), 1× TE + 50 mM NaCl. Chromatin was eluted and treated with RNaseA and Proteinase K. ChIP DNA was purified using QIAquick PCR Purification Kit (Qiagen).

Crosslink ChIP

WT and H3.3 KO ESCs were harvested and crosslinked with 1% formaldehyde in PBS for 10 min at room temperature. Crosslinking was quenched with 125 mM glycine. Cells were lysed (50 mM HEPES, pH 7.5, 140 mM NaCl, 1 mM EDTA, 10% glycerol, 0.5% NP-40, 0.25% Triton X-100), and nuclei were resuspended in ChIP buffer (10 mM Tris, pH 8, 100 mM NaCl, 1 mM EDTA, 0.5 mM EGTA, 0.1% sodium deoxycholate, 0.5% N-lauroylsarcosine). Chromatin was sonicated to an average size of 0.3–1 kb using a Covaris M220 Focused-ultrasonicator. Fifty nanograms spike-in chromatin (Active Motif 53083) was added to the soluble fraction and incubated with 50 µl Protein A Dynabeads (Invitrogen) bound to 5 µg of BRD4 antibody (Bethyl A301-985A50) and 2 µg spike-in antibody (Active Motif 61686) overnight at 4 °C. Dynabeads were washed once with each of the following: low-salt wash buffer (10 mM Tris-HCl, pH 8, 2 mM EDTA, 0.1% SDS, 1% Triton X-100, 150 mM NaCl), high-salt wash buffer (10 mM Tris-HCl, pH 8, 2 mM EDTA, 0.1% SDS, 1% Triton X-100, 500 mM NaCl), LiCl wash buffer (10 mM Tris-HCl, pH 8, 1 mM EDTA, 1% NP-40, 1% Na-Deoxycholate, 250 mM LiCl), and a final wash with TE + 50 mM NaCl. Chromatin was eluted, incubated overnight at 65 °C, and treated with RNase A and proteinase K, and DNA was purified using QIAquick PCR Purification Kit (Qiagen).

ChIP-seq library preparation

ChIP-seq libraries were prepared from 5 to 10 ng ChIP DNA following the Illumina TruSeq protocol. The quality of the libraries was assessed using a D1000 ScreenTape on a 2200 TapeStation (Agilent) and quantified using a Qubit dsDNA HS Assay Kit (Thermo Fisher). Libraries with unique adaptor barcodes were multiplexed and sequenced on an Illumina NextSeq 500 (paired-end, 50 base pair reads). Typical sequencing depth was at least 20 million reads per sample.

ChIP-seq analysis

Quality of ChIP-seq datasets was assessed using the FastQC tool. ChIP-seq raw reads were aligned separately to the mouse reference genome (mm10) and the spike-in drosophila reference genome (dm3) using BWA [78]. Only one alignment is reported for each read (either the single best alignment or, if more than one equivalent best alignment was found, one of those matches selected randomly). Duplicate reads were filtered using Picard. Uniquely mapped drosophila reads were counted in the sample containing the least number of drosophila mapped reads and used to generate a normalization factor for random downsampling. Reads were converted into bigWig files using BEDTools [78, 79] for visualization in Integrative Genomics Viewer [80]. Peak calling was performed with MACS2 software [81] using a p-value cutoff of 0.01. Heatmaps and average profiles were generated using deepTools. Box plots and density plots representing ChIP-seq read densities and fold-changes in read densities, respectively, were generated using custom R script.

CUT&Tag

CUT&Tag [49] was performed with adjustments made for crosslinking. Briefly, 3.25×10^5 nuclei were cryopreserved in Wash125 (20 mM HEPES pH 7.5, 125 mM NaCl, 10 mM NaButyrate, 0.025% Digitonin, protease inhibitor cocktail (Roche), 0.5 mM Spermidine) + 10% DMSO then stored in liquid nitrogen until experiment. Nuclei were bound to CUTANA Concanavalin A Beads (Epicypher 21-1401) for 15 min, then incubated with 50 µL Wash125 + 0.1% BSA, 2 mM EDTA, and 1 µL primary antibody overnight at 4 °C. Nuclei were resuspended in 100 µL Wash125 + 1 µL secondary antibody at room temperature for 1 h. Nuclei were washed twice in 1 mL Wash125 (with no Spermidine), then resuspended in 200 µL Wash125 - Spermidine and + 0.2% formaldehyde for 2 min and then quenched with 50 µL 2.5 M glycine. Nuclei were washed once in 1 mL Wash350 (20 mM HEPES pH 7.5, 350 mM NaCl, 10 mM NaButyrate, 0.025% Digitonin, protease inhibitor cocktail (Roche), 0.5 mM Spermidine) then incubated in 47.5 µL Wash350 + 2.5 µL pAG-Tn5 (Epicypher 15-1017) for 1 h. Nuclei were washed twice in 1 mL Wash350, then resuspended in 300 µL Wash350 + 10 mM $MgCl_2$ and incubated for 1 h at 37 °C. Tn5 reaction was stopped with 10 µL 0.5 M EDTA, 3 µL 10% SDS, and 3 µL 18 mg/mL Proteinase K, briefly vortexed, then incubated at 55 °C for 2 h to reverse crosslinks and release fragments. The fragments were then purified with phenol-chloroform and resuspended in 22 µL 1 mM Tris-HCl pH 8, 0.1 mM EDTA. The entire sample was amplified with Nextera i5 and i7 primers according to the Illumina protocol. The quality of the libraries was assessed using a D1000 ScreenTape on a 2200 TapeStation (Agilent) and quantified using a Qubit dsDNA HS Assay Kit (Thermo Fisher). Libraries with unique adaptor barcodes were multiplexed and sequenced on an Illumina NextSeq 500 (paired-end, 50 base pair reads). Typical sequencing depth was at least 15 million reads per sample.

CUT&Tag analysis

Quality of reads was assessed using the FastQC tool. Raw reads were adapter and quality trimmed using Trimgalore [82]. Trimmed reads were aligned to the mouse reference genome (mm10) with Bowtie2 [83] (bowtie2 -q -R 3 -N 1 -L 20 -i S,1,0.50 --end-to-end --dovetail --no-mixed -X 2000). Multimapping reads were randomly assigned. Optical duplicate reads were filtered using Picard. Reads which mapped to the mitochondrial genome were removed with Samtools [78]. Peak calling was performed with MACS2 software [81], and an FDR cutoff of 0.001 was applied to generate peak bedfiles. Peaks which intersected blacklisted high-signal genomic regions were removed. BigWig files were generated from alignments using deepTools [84] and normalized to counts per million (CPM). Average profiles were generated using deepTools.

ATAC-Seq

10^5 cells were lysed with ATAC buffer (Tris 10 mM, pH 7.4, 10 mM NaCl, 3 mM $MgCl_2$, NP-40 0.1%), and nuclei were collected for tagmentation at 37 °C for 30 min. The reaction was stopped with 0.2% SDS, and DNA was purified using Qiaquick PCR Purification Kit (Qiagen) and eluted in 10 µl water. Eluted DNA was amplified using

NEBNext Ultra II PCR Master Mix (NEB) and purified using AMPure XP beads. Samples were pooled for multiplexing and sequenced using paired-end sequencing on the Illumina NextSeq 500.

ATAC-seq analysis

ATAC-seq datasets for H3.3 KO, HIRA KO, ATRX KO, DAXX KO, and corresponding WT cells were obtained from GEO (GSE151013) [46]. FastQ reads were trimmed and adapters removed using Trimgalore and Cutadapt. Quality of reads was assessed using FastQC. ATAC-seq reads were aligned to the mouse reference genome (mm10) using Bowtie2 [83]. Optical duplicates were removed using Picard and reads which mapped to the mitochondrial were filtered out. Peak calling was performed using MACS2 software [81] with a *p*-value cutoff of 0.01. Peaks were further filtered to remove blacklisted regions using BEDTools [79]. A merged peak file containing all filtered ATAC peaks in every sample was used for downstream TOBIAS analysis. MACS2 was further used to generate bedgraph files which were normalized to signal per million reads. UCSC-userApps was used to convert bedgraphs to bigWigs for visualization in IGV [80]. Heatmaps and average profiles were generated from bigWig files using deepTools [84]. Differentially accessible peaks were identified using the DiffBind package [45].

Motif analysis

Active genes and expressed transcription factors were identified from RNA-seq [25] using a cutoff of >20 baseMean from DESeq2. Frequency matrices for each TF motif were downloaded from JASPAR database [85]. The TSS for active genes was downloaded as a bedfile from UCSC Table Browser and further expanded to 3 kb on either side. ATAC-seq peaks that intersected TSS beds were identified as promoter-proximal. Motifs within promoter-proximal ATAC peaks were identified using FIMO [86].

NucleoATAC analysis

For NucleoATAC analysis, replicate bam files were merged and normalized to the same sequencing depth using Samtools. Nucleosome positioning profiles were generated from merged bam files around active promoter regions (TSS ± 1 kb) with default setting of nucleoATAC. Genome browser tracks were generated converting nucleoatac_signal.smooth.bedgraph to bigwig format using bedGraphToBigWig.

Tobias analysis

For TOBIAS analysis, replicate bam files were merged. TOBIAS ATACorrect and ScoreBigWig were used to generate scored bigWig files for each merged sample across the merged ATAC peaks bedfile. BINDetect was then used to generate pairwise differential binding scores between samples for each expressed JASPAR motif. For analysis of differential binding scores specifically in promoters, BINDetect was restricted using option --output-peaks to active promoter regions (TSS ± 3 kb).

Global run-on sequencing (GRO-seq)

ESCs were lysed in Hypotonic Lysis Buffer [10 mM Tris pH 7.4, 0.5% NP-40, 10% glycerol, 3 mM $CaCl_2$, 2 mM $MgCl_2$, 1 mM DTT, 1× protease inhibitor cocktail (Roche), and

SUPERase-In (Thermo Fisher)]. Nuclei were collected by centrifugation, washed once with 1 mL Lysis Buffer, and resuspended in 500 µL of Freezing Buffer (50 mM Tris pH 8.3, 40% glycerol, 5 mM $MgCl_2$, 0.1 mM EDTA, and 4 units/mL of SUPERase-In per mL) and stored at −80 °C.

For nuclear run-on, 5×10^6 nuclei in 100 µl Freezing Buffer were mixed with an equal volume of 2X Run-on mastermix [(10 mM Tris pH 8.0, 2.5 mM $MgCl_2$, 0.5 mM DTT, 150 mM KCl, 0.25 mM rATP, 0.25 mM rGTP, 1 µM rCTP, 0.25 mM bromo-UTP, 1% sarkosyl and 0.1 U/µl SUPERase-In (Thermo Fisher)] and incubated at 30 °C for 5 min. The reaction was stopped by treatment with DNaseI and Proteinase K. NaCl was added to 225 mM, and the reaction was extracted twice with acid phenol:chloroform and once with chloroform. Following precipitation, RNA was hydrolyzed with 1N NaOH for 15 min on ice and treated with DNaseI and PNK. Fragmented RNA was bound to anti-BrdU beads in binding buffer [37.5 mM NaCl, 1 mm EDTA, 0.05% Tween, 0.25× saline-sodium-phosphate-EDTA buffer (SSPE)] for 1 h at room temperature. Beads were washed once with binding buffer, low-salt wash buffer (0.2X SSPE, 1 mM EDTA, 0.05% Tween), and high-salt wash buffer (0.25X SSPE, 1 mM EDTA, 0.05% Tween, 137.5 mM NaCl), followed by two washes in TET buffer (TE + 0.05 mM Tween). RNA was eluted 4× with elution buffer (50 mM Tris pH 7.5, 150 mM NaCl, 1 mM EDTA, 20 mM DTT, 0.1% SDS) and extracted with acid phenol:chloroform. The resulting RNAs were reverse transcribed, size-selected, and amplified. The quality of the libraries was assessed using a D1000 ScreenTape on a 2200 TapeStation (Agilent) and quantified using a Qubit dsDNA HS Assay Kit (Thermo Fisher). Libraries with unique adaptor barcodes were multiplexed and sequenced on an Illumina NextSeq 500.

GRO-seq analysis

Quality control for the GRO-seq data was performed using the FastQC tool. GRO-seq reads were trimmed to remove adapter contamination and poly(A) tails using the default parameters of Cutadapt software (Martin 2011). Reads >32 bp long were retained for alignment to the mouse reference genome. Transcript calling was performed using groHMM.

RNA-seq analysis

RNA-seq datasets used for this study were obtained from the GEO (GSE114549). Quality of raw RNA-seq reads was assessed using the FastQC tool. Reads were aligned to the mouse reference genome (mm10) with STAR [87]. After normalization, the reads were converted into bigWig files using BEDTools [79] for visualization in Integrative Genomics Viewer or the UCSC genome browser. Count matrices were generated using the featureCounts tool [88] and differential expression analysis was performed using DESeq2 (version 1.14.1) with FDR cutoff $p<0.05$.

MA plots

For each comparison, the mean of normalized counts and the $\log_2$ fold change of read counts in each gene were determined using DESeq2. These values were plotted on the x-axis and y-axis respectively for all transcripts detected. To visualize changes in

expression of genes thought to play a role in pluripotency, mouse homologs of genes included in the core ESC-like gene module [58], or PluriNet [59] were highlighted.

Western blotting

ESCs were lysed with micrococcal nuclease (Worthington) in 50 mM Tris pH 7.5, 1 mM $CaCl_2$, 0.2% Triton X-100, and 5 mM sodium butyrate. Proteins from whole cell lysate were separated in Laemmli buffer by SDS-PAGE and transferred to PVDF membranes (Millipore). Membranes were blocked in 5% milk in Tris-buffered saline with 0.1% Tween-20 (TBST) and incubated with primary antibodies overnight at 4 °C or for 2 h at room temperature. Membranes were washed with TBST, incubated with HRP-conjugated secondary antibodies for 1 h, incubated with HRP substrate (Fisher), and imaged using a ChemiDoc MP Imaging System (BioRad).

Supplementary Information

The online version contains supplementary material available at https://doi.org/10.1186/s13059-023-02867-3.

Additional file 1: Fig. S1. Loss of H3.3 deposition modestly reduces chromatin accessibility at enhancers. **Fig. S2.** HIRA facilitates H3.3 deposition at enhancers and promoters. **Fig. S3.** Loss of HIRA-mediated H3.3 deposition reduces chromatin accessibility at promoters. **Fig. S4.** HIRA-dependent loss of H3.3 deposition alters promoter architecture. **Fig. S5.** H3.3-dependent promoters display hallmarks of active chromatin. **Fig. S6.** ATRX/DAXX-dependent loss of H3.3 deposition increases accessibility at IAPEz. **Fig. S7.** Reduced ATAC-seq footprinting in the absence of H3.3. **Fig. S8.** Loss of HIRA phenocopies promoter dysregulation. **Fig. S9.** Altered H3.3 deposition influences TF binding at repeat elements. **Fig. S10.** Changes in promoter architecture are not correlated with transcriptional changes in associated proteins. **Fig. S11.** Chromatin Landsacpe Is Dysregulated with H3.3 Loss. **Fig. S12.** Loss of H3.3 alters RNAPII activty. **Fig. S13.** Transcriptional changes associated with loss of H3.3 in ESCs and during differentiation. **Fig. S14.** Uncropped blots from Fig. 6. **Fig. S15.** Exogenously expressed TFs bind at both open and closed chromatin in WT ESCs.

Additional file 2: Table S1. Pairwise comparison of TF binding activity between WT and H3.3 KO, HIRA KO, ATRX KO and DAXX KO ESCs.

Additional file 3: Table S2. Summary of pairwise comparisons of differential expression and binding activity of TFs between WT and H3.3 KO or HIRA KO ESCs.

Additional file 4: Table S3. Pairwise comparison of TF binding activity between WT ESCs and EBs or between WT and H3.3 KO EBs.

Additional file 5: Table S4. Summary of datasets generated or used in this study.

Additional file 6. Review history.

Acknowledgements

We thank members of the Banaszynski lab for feedback on this project. We thank UTSW BioHPC for computational infrastructure and UTSW McDermott Center for providing next-generation sequencing services.

Peer review information

Andrew Cosgrove was the primary editor of this article and managed its editorial process and peer review in collaboration with the rest of the editorial team.

Review history

The review history is available as Additional file 6.

Authors' contributions

A.T., R.O., and S.M. contributed equally to this work. A.T., R.O., S.M., and L.A.B. conceived and developed the project. A.T., R.O., S.M., and L.A.B. designed the experiments and oversaw their execution, with assistance from A.L.D., P.S., and V.U.G. A.T. and S.M. performed the ATAC-seq, ChIP-seq, and GRO-seq experiments. R.O. performed the CUT&Tag experiments. A.T., R.O., and S.M. analyzed the data and performed integrative analysis of genomic data sets. A.T. prepared the initial draft of the text, which was edited by R.O., finalized by L.A.B., and approved by all co-authors. L.A.B secured funding for the project and provided intellectual support for all aspects of the work. All author(s) read and approved the final manuscript.

Authors' Twitter handles

Twitter handle: @BanaszynskiLab (Laura A. Banaszynski).

Funding
L.A.B is a Virginia Murchison Linthicum Scholar in Medical Research (UTSW Endowed Scholars Program). This work was supported in part by the Welch Foundation (1-2025); the American Cancer Society (134230-RSG-20-043-01-DMC); NIH (R35 GM124958 and R01 HD109239); and the Cecil H. and Ida Green Center for Reproductive Biology Sciences. A.T. was funded by CPRIT RP160157. S.M. was a fellow of the American-Italian Cancer Foundation and the UT Southwestern Medical Center Hamon Center for Regenerative Science and Medicine.

Availability of data and materials
Code availability Code to generate figures is available at https://github.com/utsw-medical-center-banaszynski-lab/Tafessu-et-al-2023-GenomeBiology.
Data availability Datasets are deposited in the NCBI Gene Expression Omnibus using the following accession numbers: SuperSeries GSE186687, ATAC-seq GSE186684, ChIP-seq GSE186685, GRO-seq GSE186686, and CUT&Tag GSE213039 [89]. Other datasets used for this study are available under GSE114551 [25, 90] and GSE151058 [46, 91]. For data used in individual figure panels, see Additional file 5: Table S4.

Declarations

Ethics approval and consent to participate
Not applicable.

Consent for publication
Not applicable.

Competing interests
The authors declare that they have no competing interests.

Received: 19 November 2021 Accepted: 6 February 2023
Published online: 13 February 2023

References

1. Kornberg RD. Chromatin structure: a repeating unit of histones and DNA. Science. 1974;184:868–71.
2. Luger K, Mäder AW, Richmond RK, Sargent DF, Richmond TJ. Crystal structure of the nucleosome core particle at 2.8 Å resolution. Nature. 1997:251–60. https://doi.org/10.1038/38444.
3. Allis CD, Jenuwein T. The molecular hallmarks of epigenetic control. Nat Rev Genet. 2016;17:487–500.
4. Klemm SL, Shipony Z, Greenleaf WJ. Chromatin accessibility and the regulatory epigenome. Nat Rev Genet. 2019;20:207–20.
5. Zaret KS. Pioneer transcription factors initiating gene network changes. Annu Rev Genet. 2020;54:367–85.
6. Clapier CR, Iwasa J, Cairns BR, Peterson CL. Mechanisms of action and regulation of ATP-dependent chromatin-remodelling complexes. Nat Rev Mol Cell Biol. 2017;18:407–22.
7. Martire S, Banaszynski LA. The roles of histone variants in fine-tuning chromatin organization and function. Nat Rev Mol Cell Biol. 2020;21:522–41.
8. Jin C, Felsenfeld G. Nucleosome stability mediated by histone variants H3.3 and H2A.Z. Genes Dev. 2007:1519–29. https://doi.org/10.1101/gad.1547707.
9. Jin C, Zang C, Wei G, Cui K, Peng W, Zhao K, et al. H3.3/H2A.Z double variant–containing nucleosomes mark "nucleosome-free regions" of active promoters and other regulatory regions. Nat Genet. 2009:941–5. https://doi.org/10.1038/ng.409.
10. Giaimo BD, Ferrante F, Herchenröther A, Hake SB, Borggrefe T. The histone variant H2A.Z in gene regulation. Epigenetics Chromatin. 2019;12:37.
11. Hu G, Cui K, Northrup D, Liu C, Wang C, Tang Q, et al. H2A.Z facilitates access of active and repressive complexes to chromatin in embryonic stem cell self-renewal and differentiation. Cell Stem Cell. 2013;12:180–92 Elsevier Inc.
12. Murphy KE, Meng FW, Makowski CE, Murphy PJ. Genome-wide chromatin accessibility is restricted by ANP32E. Nat Commun. 2020;11:5063.
13. Tafessu A, Banaszynski LA. Establishment and function of chromatin modification at enhancers. Open Biol. 2020;10:200255.
14. Ahmad K, Henikoff S. The histone variant H3.3 marks active chromatin by replication-independent nucleosome assembly. Mol Cell. 2002;9:1191–200.
15. Goldberg AD, Banaszynski LA, Noh K-M, Lewis PW, Elsaesser SJ, Stadler S, et al. Distinct factors control histone variant H3.3 localization at specific genomic regions. Cell. 2010;140:678–91.
16. Mito Y, Henikoff JG, Henikoff S. Genome-scale profiling of histone H3.3 replacement patterns. Nat Genet. 2005;37:1090–7.
17. Ray-Gallet D, Woolfe A, Vassias I, Pellentz C, Lacoste N, Puri A, et al. Dynamics of histone H3 deposition in vivo reveal a nucleosome gap-filling mechanism for H3.3 to maintain chromatin integrity. Mol Cell. 2011;44:928–41.
18. Ha M, Kraushaar DC, Zhao K. Genome-wide analysis of H3.3 dissociation reveals high nucleosome turnover at distal regulatory regions of embryonic stem cells. Epigenetics Chromatin. 2014;7:38.
19. Schlesinger S, Kaffe B, Melcer S, Aguilera JD, Sivaraman DM, Kaplan T, et al. A hyperdynamic H3.3 nucleosome marks promoter regions in pluripotent embryonic stem cells. Nucleic Acids Res. 2017;45:12181–94.
20. Deaton AM, Gómez-Rodríguez M, Mieczkowski J, Tolstorukov MY, Kundu S, Sadreyev RI, et al. Enhancer regions show high histone H3.3 turnover that changes during differentiation. Elife. 2016:5. https://doi.org/10.7554/eLife.15316.

21. Schneiderman JI, Orsi GA, Hughes KT, Loppin B, Ahmad K. Nucleosome-depleted chromatin gaps recruit assembly factors for the H3.3 histone variant. Proc Natl Acad Sci U S A. 2012;109:19721–6.
22. Thakar A, Gupta P, Ishibashi T, Finn R, Silva-Moreno B, Uchiyama S, et al. H2A.Z and H3.3 histone variants affect nucleosome structure: biochemical and biophysical studies. Biochemistry. 2009;48:10852–7.
23. Flaus A, Rencurel C, Ferreira H, Wiechens N, Owen-Hughes T. Sin mutations alter inherent nucleosome mobility. EMBO J. 2004;23:343–53.
24. Tachiwana H, Osakabe A, Shiga T, Miya Y, Kimura H, Kagawa W, et al. Structures of human nucleosomes containing major histone H3 variants. Acta Crystallogr D Biol Crystallogr. 2011;67:578–83.
25. Martire S, Gogate AA, Whitmill A, Tafessu A, Nguyen J, Teng Y-C, et al. Phosphorylation of histone H3.3 at serine 31 promotes p300 activity and enhancer acetylation. Nat Genet. 2019;51:941–6.
26. Navarro C, Lyu J, Katsori A-M, Caridha R, Elsässer SJ. An embryonic stem cell-specific heterochromatin state promotes core histone exchange in the absence of DNA accessibility. Nat Commun. 2020;11:5095.
27. Kraushaar DC, Chen Z, Tang Q, Cui K, Zhang J, Zhao K. The gene repressor complex NuRD interacts with the histone variant H3.3 at promoters of active genes. Genome Res. 2018;28:1646–55 genome.cshlp.org.
28. Elsässer SJ, Noh K-M, Diaz N, Allis CD, Banaszynski LA. Histone H3.3 is required for endogenous retroviral element silencing in embryonic stem cells. Nature. 2015;522:240–4.
29. Banaszynski LA, Wen D, Dewell S, Whitcomb SJ, Lin M, Diaz N, et al. Hira-dependent histone H3.3 deposition facilitates PRC2 recruitment at developmental loci in ES cells. Cell. 2013;155:107–20.
30. Gehre M, Bunina D, Sidoli S, Lübke MJ, Diaz N, Trovato M, et al. Lysine 4 of histone H3.3 is required for embryonic stem cell differentiation, histone enrichment at regulatory regions and transcription accuracy. Nat Genet. 2020;52:273–82 Nature Publishing Group.
31. Heintzman ND, Hon GC, Hawkins RD, Kheradpour P, Stark A, Harp LF, et al. Histone modifications at human enhancers reflect global cell-type-specific gene expression. Nature. 2009;459:108–12.
32. Sitbon D, Boyarchuk E, Dingli F, Loew D, Almouzni G. Histone variant H3.3 residue S31 is essential for Xenopus gastrulation regardless of the deposition pathway. Nat Commun. 2020;11:1256.
33. Zhang T, Zhang Z, Dong Q, Xiong J, Zhu B. Histone H3K27 acetylation is dispensable for enhancer activity in mouse embryonic stem cells. Genome Biol. 2020;21:45.
34. Kong Q, Banaszynski LA, Geng F, Zhang X, Zhang J, Zhang H, et al. Histone variant H3.3-mediated chromatin remodeling is essential for paternal genome activation in mouse preimplantation embryos. J Biol Chem. 2018;293:3829–38.
35. Nashun B, Hill PWS, Smallwood SA, Dharmalingam G, Amouroux R, Clark SJ, et al. Continuous histone replacement by HIRA is essential for normal transcriptional regulation and de novo DNA methylation during mouse oogenesis. Mol Cell. 2015;60:611–25.
36. Armache A, Yang S, de Paz AM, Robbins LE, Durmaz C, Cheong JQ, et al. Histone H3.3 phosphorylation amplifies stimulation-induced transcription. Nature. 2020:583, 852–7. https://doi.org/10.1038/s41586-020-2533-0.
37. Zhang H, Gan H, Wang Z, Lee J-H, Zhou H, Ordog T, et al. RPA interacts with HIRA and regulates H3.3 deposition at gene regulatory elements in mammalian cells. Mol Cell. 2017;65:272–84.
38. Kim H, Heo K, Choi J, Kim K, An W. Histone variant H3.3 stimulates HSP70 transcription through cooperation with HP1γ. Nucleic Acids Res. 2011;39:8329–41.
39. Tamura T, Smith M, Kanno T, Dasenbrock H, Nishiyama A, Ozato K. Inducible Deposition of the Histone Variant H3.3 in Interferon-stimulated Genes. J Biol Chem. 2009:12217–25. https://doi.org/10.1074/jbc.m805651200.
40. Gomes AP, Ilter D, Low V, Rosenzweig A, Shen Z-J, Schild T, et al. Dynamic incorporation of histone H3 variants into chromatin is essential for acquisition of aggressive traits and metastatic colonization. Cancer Cell. 2019;36:402–17. e13.
41. Jang C-W, Shibata Y, Starmer J, Yee D, Magnuson T. Histone H3.3 maintains genome integrity during mammalian development. Genes Dev. 2015;29:1377–92.
42. Sakai A, Schwartz BE, Goldstein S, Ahmad K. Transcriptional and developmental functions of the H3.3 histone variant in Drosophila. Curr Biol. 2009;19:1816–20.
43. Hödl M, Basler K. Transcription in the absence of histone H3. 3. Curr Biol. 2009;19:1221–6 Elsevier.
44. Schep AN, Buenrostro JD, Denny SK, Schwartz K, Sherlock G, Greenleaf WJ. Structured nucleosome fingerprints enable high-resolution mapping of chromatin architecture within regulatory regions. Genome Res. 2015;25:1757–70.
45. Stark R, Brown G, Others. DiffBind: differential binding analysis of ChIP-Seq peak data. R package version; 2011. p. 100. Available from: http://bioconductor.statistik.tu-dortmund.de/packages/2.13/bioc/vignettes/DiffBind/inst/doc/DiffBind.pdf
46. Teng Y-C, Sundaresan A, O'Hara R, Gant VU, Li M, Martire S, et al. ATRX promotes heterochromatin formation to protect cells from G-quadruplex DNA-mediated stress. Nat Commun. 2021;12:3887.
47. Bentsen M, Goymann P, Schultheis H, Klee K, Petrova A, Wiegandt R, et al. ATAC-seq footprinting unravels kinetics of transcription factor binding during zygotic genome activation. Nat Commun. 2020;11:4267.
48. Chambers I, Tomlinson SR. The transcriptional foundation of pluripotency. Development. 2009;136:2311–22.
49. Kaya-Okur HS, Wu SJ, Codomo CA, Pledger ES, Bryson TD, Henikoff JG, et al. CUT&Tag for efficient epigenomic profiling of small samples and single cells. Nat Commun. 2019;10:1930.
50. Dancy BM, Cole PA. Protein lysine acetylation by p300/CBP. Chem Rev. 2015;115:2419–52.
51. Cenik BK, Shilatifard A. COMPASS and SWI/SNF complexes in development and disease. Nat Rev Genet. 2021;22:38–58.
52. Spitz F, Furlong EEM. Transcription factors: from enhancer binding to developmental control. Nat Rev Genet. 2012;13:613–26.
53. Fang L, Zhang J, Zhang H, Yang X, Jin X, Zhang L, et al. H3K4 methyltransferase Set1a is a key Oct4 coactivator essential for generation of Oct4 positive inner cell mass. Stem Cells. 2016;34:565–80.
54. Muntean AG, Tan J, Basrur V, Elenitoba-Johnson KSJ, Hess J. The PAF complex synergizes with MLL fusion proteins at .Hox loci to promote leukemogenesis. Blood. 2009:1277. https://doi.org/10.1182/blood.v114.22.1277.1277.

55. Merika M, Williams AJ, Chen G, Collins T, Thanos D. Recruitment of CBP/p300 by the IFNβ enhanceosome is required for synergistic activation of transcription. Mol Cell. 1998;1:277–87.
56. Kanno T, Kanno Y, LeRoy G, Campos E, Sun H-W, Brooks SR, et al. BRD4 assists elongation of both coding and enhancer RNAs by interacting with acetylated histones. Nat Struct Mol Biol. 2014;21:1047–57.
57. Wissink EM, Vihervaara A, Tippens ND, Lis JT. Nascent RNA analyses: tracking transcription and its regulation. Nat Rev Genet. 2019;20:705–23.
58. Wong DJ, Liu H, Ridky TW, Cassarino D, Segal E, Chang HY. Module map of stem cell genes guides creation of epithelial cancer stem cells. Cell Stem Cell. 2008;2:333–44.
59. Müller F-J, Laurent LC, Kostka D, Ulitsky I, Williams R, Lu C, et al. Regulatory networks define phenotypic classes of human stem cell lines. Nature. 2008;455:401–5.
60. Tsankov AM, Gu H, Akopian V, Ziller MJ, Donaghey J, Amit I, et al. Transcription factor binding dynamics during human ES cell differentiation. Nature. 2015;518:344–9.
61. Takahashi K, Yamanaka S. Induction of pluripotent stem cells from mouse embryonic and adult fibroblast cultures by defined factors. Cell. 2006;126:663–76.
62. Michael AK, Grand RS, Isbel L, Cavadini S, Kozicka Z, Kempf G, et al. Mechanisms of OCT4-SOX2 motif readout on nucleosomes. Science. 2020;368:1460–5.
63. King HW, Klose RJ. The pioneer factor OCT4 requires the chromatin remodeller BRG1 to support gene regulatory element function in mouse embryonic stem cells. Elife. 2017;6. https://doi.org/10.7554/eLife.22631.
64. Singhal N, Graumann J, Wu G, Araúzo-Bravo MJ, Han DW, Greber B, et al. Chromatin-remodeling components of the BAF complex facilitate reprogramming. Cell. 2010;141:943–55.
65. Barisic D, Stadler MB, Iurlaro M, Schübeler D. Mammalian ISWI and SWI/SNF selectively mediate binding of distinct transcription factors. Nature. 2019;569:136–40.
66. Fang H-T, El Farran CA, Xing QR, Zhang L-F, Li H, Lim B, et al. Global H3.3 dynamic deposition defines its bimodal role in cell fate transition. Nat Commun. 2018;9:1537.
67. Leatham-Jensen M, Uyehara CM, Strahl BD, Matera AG, Duronio RJ, McKay DJ. Lysine 27 of replication-independent histone H3.3 is required for Polycomb target gene silencing but not for gene activation. PLoS Genet. 2019;15:e1007932 journals.plos.org.
68. Martire S, Nguyen J, Sundaresan A, Banaszynski LA. Differential contribution of p300 and CBP to regulatory element acetylation in mESCs. BMC Mol Cell Biol. 2020;21:55.
69. Morgan MAJ, Shilatifard A. Reevaluating the roles of histone-modifying enzymes and their associated chromatin modifications in transcriptional regulation. Nat Genet. 2020;52:1271–81.
70. Aubert Y, Egolf S, Capell BC. The unexpected noncatalytic roles of histone modifiers in development and disease. Trends Genet. 2019;35:645–57.
71. Rickels R, Herz H-M, Sze CC, Cao K, Morgan MA, Collings CK, et al. Histone H3K4 monomethylation catalyzed by Trr and mammalian COMPASS-like proteins at enhancers is dispensable for development and viability. Nat Genet. 2017:1647–53. https://doi.org/10.1038/ng.3965.
72. Dorighi KM, Swigut T, Henriques T, Bhanu NV, Scruggs BS, Nady N, et al. Mll3 and Mll4 facilitate enhancer RNA synthesis and transcription from promoters independently of H3K4 monomethylation. Mol Cell. 2017;66:568–76.e4.
73. Whyte WA, Bilodeau S, Orlando DA, Hoke HA, Frampton GM, Foster CT, et al. Enhancer decommissioning by LSD1 during embryonic stem cell differentiation. Nature. 2012;482:221–5.
74. Schwartzentruber J, Korshunov A, Liu X-Y, Jones DTW, Pfaff E, Jacob K, et al. Driver mutations in histone H3.3 and chromatin remodelling genes in paediatric glioblastoma. Nature. 2012;482:226–31.
75. Behjati S, Tarpey PS, Presneau N, Scheipl S, Pillay N, Van Loo P, et al. Distinct H3F3A and H3F3B driver mutations define chondroblastoma and giant cell tumor of bone. Nat Genet. 2013;45:1479–82.
76. Bryant L, Li D, Cox SG, Marchione D, Joiner EF, Wilson K, et al. Histone H3.3 beyond cancer: Germline mutations in Histone 3 Family 3A and 3B cause a previously unidentified neurodegenerative disorder in 46 patients. Sci Adv. 2020;6. https://doi.org/10.1126/sciadv.abc9207.
77. Sadic D, Schmidt K, Groh S, Kondofersky I, Ellwart J, Fuchs C, et al. Atrx promotes heterochromatin formation at retrotransposons. EMBO Rep. 2015:836–50. https://doi.org/10.15252/embr.201439937.
78. Li H, Durbin R. Fast and accurate short read alignment with Burrows-Wheeler transform. Bioinformatics. 2009;25:1754–60.
79. Quinlan AR, Hall IM. BEDTools: a flexible suite of utilities for comparing genomic features. Bioinformatics. 2010;26:841–2.
80. Robinson JT, Thorvaldsdóttir H, Winckler W, Guttman M, Lander ES, Getz G, et al. Integrative genomics viewer. Nat Biotechnol. 2011;29:24–6.
81. Zhang Y, Liu T, Meyer CA, Eeckhoute J, Johnson DS, Bernstein BE, et al. Model-based analysis of ChIP-Seq (MACS). Genome Biol. 2008;9:R137.
82. Krueger F. Trim Galore: a wrapper tool around Cutadapt and FastQC to consistently apply quality and adapter trimming to FastQ files, with some extra functionality for MspI-digested RRBS-type. 2012 (Reduced Representation Bisufite-Seq) libraries. http://www.bioinformatics.babraham.ac.uk/projects/trim_galore/ (Date of access: 28 Apr 2016).
83. Langmead B, Salzberg SL. Fast gapped-read alignment with Bowtie 2. Nat Methods. 2012;9:357–9.
84. Ramírez F, Ryan DP, Grüning B, Bhardwaj V, Kilpert F, Richter AS, et al. deepTools2: a next generation web server for deep-sequencing data analysis. Nucleic Acids Res. 2016;44:W160–5.
85. Fornes O, Castro-Mondragon JA, Khan A, van der Lee R, Zhang X, Richmond PA, et al. JASPAR 2020: update of the open-access database of transcription factor binding profiles. Nucleic Acids Res. 2019. https://doi.org/10.1093/nar/gkz1001.
86. Grant CE, Bailey TL, Noble WS. FIMO: scanning for occurrences of a given motif. Bioinformatics. 2011:1017–8. https://doi.org/10.1093/bioinformatics/btr064.
87. Dobin A, Davis CA, Schlesinger F, Drenkow J, Zaleski C, Jha S, et al. STAR: ultrafast universal RNA-seq aligner. Bioinformatics. 2013;29:15–21.

88. Liao Y, Smyth GK, Shi W. featureCounts: an efficient general purpose program for assigning sequence reads to genomic features. Bioinformatics. 2014;30:923–30.
89. Tafessu A, O'Hara R, Martire S, Banaszynski LA. Histone Variant H3.3 facilitates open chromatin at promoters. ATAC-seq, ChIP-seq, GRO-seq, CUT&Tag: Gene Expression Omnibus; 2023. https://www.ncbi.nlm.nih.gov/geo/query/acc.cgi?acc=GSE186687
90. Martire S, Gogate AA, Whitmill A, Tafessu A, Nguyen J, Teng YC, et al. H3.3 phosphorylation promotes enhancer acetylation and lineage specification. ATAC-seq, ChIP-seq, RNA-seq: Gene Expression Omnibus; 2019. https://www.ncbi.nlm.nih.gov/geo/query/acc.cgi?acc=GSE114551
91. Teng Y, Sundaresan A, Banaszynski LA. ATRX promotes heterochromatin formation to protect cells from G-quadruplex DNA-mediated stress. ATAC-seq: Gene Expression Omnibus; 2021. https://www.ncbi.nlm.nih.gov/geo/query/acc.cgi?acc=GSE151058

Publisher's Note